Numerical modeling of two-phase underexpanded reactive CO_2-into-sodium jets in the frame ofSodium nuclear Fast Reactors

D. Vivaldi, F. Gruy, C. Perrais

NUMERICAL MODELING OF TWO-PHASE UNDEREXPANDED REACTIVE CO_2-INTO-SODIUM JETS IN THE FRAME OF SODIUM NUCLEAR FAST REACTORS

Daniele Vivaldi[1], Frédéric Gruy[2], Christophe Perrais[1]
[1]CEA, DEN/DTN/SMTA/LIPC Cadarache, F-13108 Saint Paul lez Durance, France
[2]Ecole Nationale Supérieure des Mines de Saint-Etienne, Centre SPIN, Département PROPICE, LGF UMR 5307
daniele.vivaldi@areva.com; fgruy@emse.fr; christophe.perrais@cea.fr

ABSTRACT

Supercritical CO_2 (sCO_2) Brayton cycles have gained interest in the frame of Sodium-cooled nuclear Fast Reactors (SFRs), as an alternative to the conventional water Rankine cycles. If CO_2 leaks inside the CO_2-Na heat exchanger, an underexpanded CO_2-into-liquid-sodium jet is formed. CO_2 leaks at sonic velocity and chemically reacts with sodium, through an exothermic reaction. The consequences of such a scenario must be investigated, in order to predict the temperature increasing inside the heat exchanger and on the tube walls, due to the exothermic chemical reaction, as well as the reaction products distribution inside the heat exchanger. This article presents a numerical approach for modeling such a two-phase reactive jet. A two-fluid multi-component CFD approach is employed, with a heterogeneous reaction between the CO_2-gas and the sodium-liquid phases. The model allows to predict the most relevant information, such as temperature distribution, the jet penetration length and the reaction products distribution downstream the CO_2 leakage. Some experimental studies on underexpanded gas-into-sodium reactive jets, available in literature, have been compared to our numerical results. It is found that the numerical temperature profiles are consistent with the ones experimentally measured.

KEYWORDS
Sodium Fast Reactors, Underexpanded two-phase jets, Multi-fluid CFD, Heterogeneous gas-liquid chemical reaction, Supercritical CO_2 cycles

1. INTRODUCTION

In SFRs, sCO_2 Brayton cycles represent an interesting alternative to water Rankine cycles [1,2,3,4], since they eliminate the wastage accidental scenario caused by the sodium water reaction [5] and feature high thermodynamic plant efficiency (up to 42% [2]). Nevertheless, CO_2 exothermically reacts with sodium, forming solid reaction products (mainly sodium carbonate and carbon). In order to fully understand the feasibility of employing sCO_2 Brayton cycles for SFRs, the consequences of the CO_2 leakage scenario must be investigated. Considering that the CO_2 and sodium operating pressure inside the heat exchanger is about 20 MPa and about 0.3 MPa, respectively, a tube leakage would result in an underexpanded CO_2-into-sodium reactive jet. A numerical approach for modeling non-reactive underexpanded gas-into-liquid jets have been already developed by the authors [6]: a two-fluid CFD approach was employed, with droplet- and bubbly-flow coexistence, depending on the local void fraction. Concerning the CO_2-sodium chemical reaction inside such a two-phase jet, a chemical reaction model has been developed by the authors: the model calculates the Na droplet and the CO_2 bubble depletion rates. In the present paper, the

modeling of the two-phase reactive jet is achieved by coupling the non-reactive underexpanded jet model and the CO_2-sodium chemical reaction model.

2. TWO-FLUID APPROACH

The numerical model described in the following will be applied to a geometry representing the sodium pool of the CO_2-into-sodium jet test facility available at CEA Cadarache [7].
The two-fluid approach solves the constitutive mass, momentum and energy equations for each phase, respectively:

$$\frac{\partial(\alpha_p \rho_p)}{\partial t} + \nabla \cdot (\alpha_p \rho_p \vec{U}_p) = S_p \tag{1}$$

$$\frac{\partial}{\partial t}(\alpha_p \rho_p \vec{U}_p) + \nabla \cdot (\alpha_p \rho_p \vec{U}_p \vec{U}_p) = -\alpha_p \nabla P + \nabla \cdot \left(\alpha_p (\mu_p + \mu_{t,p})\left(\nabla \vec{U}_p + (\nabla \vec{U}_p)^T\right)\right) + \alpha_p \rho_p \vec{g} + S_p^{\vec{U}} + \vec{F}_{pq} \tag{2}$$

$$\frac{\partial}{\partial t}(\alpha_p \rho_p h_p) + \nabla \cdot (\alpha_p \rho_p \vec{U}_p h_p) = -\alpha_p \frac{\partial P}{\partial t} + \nabla \cdot (\alpha_p (\lambda_p + \lambda_{t,p}) \nabla T_p) + S_p^H + Q_{pq} \tag{3}$$

Where ρ_p, α_p, $\vec{U}_p$ and h_p are density, volume fraction, velocity and enthalpy of the generic phase *p*, respectively. S_p is a source term taking into account mass creation of phase *p* due, for example, to chemical reactions. *P* is the static pressure shared by the two phases. μ_p and $\mu_{t,p}$ are the dynamic and turbulent viscosities, respectively. $\vec{g}$ is the gravitational acceleration, $S_p^{\vec{U}}$ represents the momentum transfer caused by heterogeneous reactions, and F_{pq} is the interfacial force source term. λ_p is the thermal conductivity of phase *p*, whereas $\lambda_{t,p}$ is the turbulent thermal conductivity. Q_{pq} is the interfacial heat transfer flux and S_p^H is the energy source term taking into account, for example, heat due to exothermic or endothermic chemical reactions.

A $k-\varepsilon$ turbulence model has been applied to the gas-liquid mixture in order to calculate the turbulent viscosity. The equations of this model are detailed in [6]. The dissipation correction term proposed by Sarkar [8] has been employed for taking into account the compressibility effect in the $k-\varepsilon$ model.
Turbulent viscosity for the phase *p* is evaluated through $\mu_{t,p} = \frac{\rho_p}{\rho_m}\mu_{t,m}$, where the mixture turbulent viscosity is calculated through $\mu_{t,m} = C_\mu \rho_m \frac{k^2}{\varepsilon}$ (ρ_m being the density of the gas-liquid mixture).

2.1. Interfacial friction and heat transfer

As detailed in [6], in order to consider both droplet and bubbly flows, the approach employed in the SIMMER-III [9,10] computational code has been adopted in the present work: droplet flow is assumed for void fractions higher than a defined value α_d, bubbly flow is assumed for void fractions lower than a defined value α_b, and a transition flow is defined by combining the two regions. Therefore, two separated drag force equations have been written depending on which flow regime characterizes the computational cell considered:

$$\vec{F}_{D,l} = -\vec{F}_{D,g} = \begin{cases} \frac{3}{4}\frac{(1-\alpha)}{d_d} C_{D,d}\rho_g \left|\vec{U}_g - \vec{U}_l\right|\left(\vec{U}_g - \vec{U}_l\right) & \text{if } \alpha \geq \alpha_d \\ \frac{3}{4}\frac{\alpha}{d_b} C_{D,b}\rho_l \left|\vec{U}_g - \vec{U}_l\right|\left(\vec{U}_g - \vec{U}_l\right) & \text{if } \alpha \leq \alpha_b \end{cases} \quad (4)$$

This is the interfacial friction which enters into the F_{pq} term. In Eq. (4), subscript *g* and *l* stand for gas and liquid phase, respectively. $C_{D,d}$ and $C_{D,b}$ are the droplet and bubble drag coefficients, respectively, d_d and d_b are the droplet and bubble diameters, respectively. In the transition flow regime between α_b and α_d, the drag law is continuously interpolated between droplet and bubble drag laws, using a logarithmic weighted average.
Similarly, for the calculation of the interfacial heat transfer flux per unit volume:

$$Q_{gl} = -Q_{lg} = a \cdot h \cdot \Delta T_{gl} \quad (5)$$

the product $a \cdot h$ (a being the interfacial area) in Eq.(5) has been evaluated assuming droplet flow for $\alpha \geq \alpha_d$, bubbly flow for $\alpha \leq \alpha_b$, and using a weighted logarithmic average for the transition flow.
For the determination of the droplet diameter, the experimental results obtained by Epstein et al. [11] and Kudoh et al. [12] have been employed: for a gas injection pressure ranging between 0.2 and 1.5 MPa and a nozzle diameter ranging from 1.0 to 2.0 mm, entrained droplet Sauter mean diameter was found to range between 10 and 50 μm. The experimental results we want to reproduce through the numerical model were obtained with an injection total pressure of 0.7 Mpa: the corresponding estimated droplet diameter (d_d) through Epstein's correlation is 20 μm. Bubble diameter has been estimated following the critical Weber number parameter: the Weber number (*We*) is the ratio between the inertial force and the surface tension force for a particle:

$$We = \frac{\rho_l \cdot \Delta\vec{U}^2 \cdot d_b}{\sigma} \quad (6)$$

Hinze and Kolmogorov [13,14] showed that the appropriate velocity term in Eq. (6) is the root mean square of the velocity difference over a distance equal to the particle (i.e. the bubble for the present case) diameter, and its value may be approximated by:

$$\Delta U^2 = 2(\varepsilon \cdot d_b)^{2/3} \quad (7)$$

Substituting Eq. (7) in Eq. (6), one obtains the following equation for the maximum particle size:

$$d_{b,\max} = \left(\frac{We_c}{2}\right)^{3/5}\left(\frac{\sigma}{\rho_l}\right)^{3/5}\varepsilon^{-2/5} \quad (8)$$

The critical Weber number (We_c) suggested by Hinze is 1.2. The value of the bubble diameter (d_b) retained in our model is 0.4 mm, which is the resulting value from Eq. (8) employing the turbulent energy dissipation rate (ε) calculated in the region where bubbly flow is supposed to generate ($\alpha = \alpha_b$), for an injection pressure of 0.7 MPa.

Following the results in [6], the droplet-flow lowest void fraction limit (α_d) was fixed equal to 0.80, and the bubbly-flow highest void fraction limit (α_b) to 0.50.

3. CHEMICAL REACTION MODEL

The following reaction path is considered [15]:

$$Na + \frac{3}{4}CO_2 \rightarrow \frac{1}{4}C + \frac{1}{2}Na_2CO_3 \quad -272\frac{kJ}{mol_{Na}} \tag{9}$$

As it can be seen, liquid sodium and gaseous carbon dioxide produce carbon and sodium carbonate. Carbon is a solid product, whereas the Na_2CO_3 fusion point is 851°C. In order not to further complicate the numerical approach, the main assumption is made that the products of reaction and liquid sodium belong to a unique condensed phase. If the solid phase had to be added as an additional dedicated field, its modeling would require to take into account the solid particle nucleation, growth and agglomeration kinetics, to be implemented into a balance of population approach coupled to the CFD approach. Beside the further complication of the numerical formulation, this is at present an impossible task because the necessary information about the elementary phenomena (nucleation, growth and agglomeration) are unknown. From the chemical reaction point of view, the solid reaction products, even if not explicitly modeled, are taken into account in the numerical chemical reaction modeled developed by the authors for the sodium droplet reaction (see [15]), since they are supposed to lie inside the droplet diffusion-reaction boundary layer and therefore to limit the quantity of Na and CO_2 available for the reaction. From the fluid-dynamics point of view, one has to consider that the density of liquid Na is in the same order of magnitude of the one of solid Na_2CO_3 and C; moreover, the solid particles have submicronic or micronic dimensions, meaning that their Stokes number is low enough to consider that they are entrained by the liquid sodium flow and, as a first approximation, they can belong to the same field.
Following this assumption, reaction (9) can be rewritten as:

$$Na + \frac{3}{4}CO_2 \rightarrow P_{liq} \quad -272\frac{kJ}{mol_{Na}} \tag{10}$$

The CO_2-Na chemical reaction model employed in the present paper is described in [15]. The model allows to calculate the depletion rate of a sodium droplet surrounded by CO_2 and of a CO_2 bubble surrounded by liquid sodium. In this way, the chemical reaction rate can be evaluated for both the mist and bubbly flow regions characterizing the two phase jet. The droplet depletion rate depends on its diameter, its relative velocity, the gas and liquid temperatures, and the chemical reaction kinetic parameters. The bubble depletion rate depends on its diameter, the gas and the liquid temperatures, and the chemical reaction kinetic parameters. The kinetic parameters are the activation energy (E_a) and pre-exponential factor (k_0) of an Arrhenius type equation:

$$k = k_0 \cdot \exp\left(\frac{-E_a}{R_g T}\right) \tag{11}$$

It is found that the following type of correlation well represents the numerical results in terms of the sodium reaction rate of the droplet, $\dot{m}_{Na,droplet}$ [15]:

$$\dot{m}_{Na,droplet}\left[\frac{kg}{s}\right]=\left(A\cdot T_{Na}^{3}+B\cdot T_{Na}^{2}+C\cdot T_{Na}+D\right)\cdot\left(Y_{CO_2,bulk}\right)^{b} \tag{12}$$

Where *A*, *B*, *C* and *D* are function of the specific kinetic parameters of the Arrhenius equation (11). T_{Na} refers to sodium (i.e. the droplet) temperature. The mass fraction $Y_{CO_2,bulk}$ surrounding the sodium droplets is evaluated, inside a computational cell, through $Y_{CO_2,bulk}=Y_{CO_2}\left(1-Y_{Na}\right)^{-1}$. It is found that the value of *b* does not change for different pre-exponential factors, and its value is equal to 0.40.
It is found that the following type of correlation well represents the numerical results in terms of CO_2 bubble reaction rate [15] (for simplicity, we always refer to the sodium reaction rate):

$$\dot{m}_{Na,droplet}\left[\frac{kg}{s}\right]=\left(A'\cdot T_{Na}^{3}+B'\cdot T_{Na}^{2}+C'\cdot T_{Na}+D'\right) \tag{13}$$

Where *A′*, *B′*, *C′* and *D′* are function of the specific kinetic parameters of the Arrhenius Eq. (11).
Depending on the actual void fraction inside each computational cell, a reaction regime can be defined, as shown in Fig. 1.

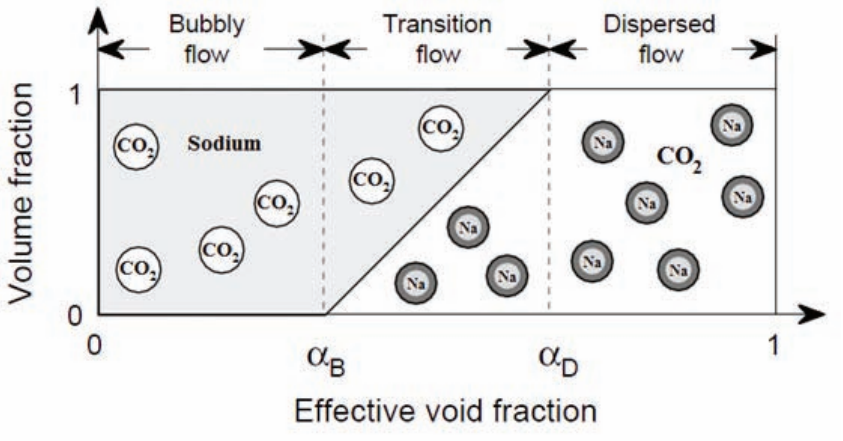

Figure 1: Heterogeneous reaction map inside a computational cell.

In order to evaluate the total reaction rate ($\dot{r}$) inside a computational cell, the total number of droplets (N_d) and bubbles (N_b) per unit volume is first calculated through the void fraction and the particle diameter. The total droplet and bubble reaction rate inside a cell can be then evaluated by Eqs. (14) and (15), respectively:

$$\dot{r}_{Na,droplet_{total}}\left[\frac{kmol}{m^3 s}\right]=\frac{N_d\cdot\dot{m}_{Na,droplet}}{M_{Na}} \tag{14}$$

$$\dot{r}_{Na,bubble_{total}}\left[\frac{kmol}{m^3 s}\right]=\frac{N_b\cdot\dot{m}_{Na,bubble}}{M_{Na}} \tag{15}$$

The reaction rate for the transition flow regime ($\alpha_b<\alpha<\alpha_d$) is estimated applying a logarithmic weighted average.

4. IMPLEMENTATION OF THE CHEMICAL REACTION INTO THE TWO-FLUID MODEL

In order to couple the chemical reaction model with the non-reactive jet model, source terms have to be added inside the two-fluid model equations (Eqs. (1), (2) and (3)). These source terms have to take into account the influence of the chemical reaction between CO_2 and Na, in terms of mass, momentum and energy production/destruction for each phase.
Employing subscripts *l* and *g* for the liquid and gas phase, respectively, and considering the stoichiometry of reaction (10), the mass source terms for the two phases will be:

$$S_l = \dot{r}\left(M_P - M_{Na}\right) \tag{16}$$

$$S_g = \dot{r}\left(-\frac{3}{4}M_{CO_2}\right) \tag{17}$$

For calculating the momentum transfer due to heterogeneous chemical reactions, $S_p^{\vec{U}}$, it is assumed that the reactants mixture and the products take momentum in the ratio of the rate of their formation.
Employing subscripts *r* and *pr* for reactants and products, respectively, and r_p and pr_p for reactants and products of phase *p*, respectively, the general expression of the net velocity, $\vec{U}_{net}$, of the reactants is given by:

$$\vec{U}_{net} = \frac{\sum_r s_r M_r \vec{U}_r}{\sum_r s_r M_r} \tag{18}$$

Where *s* is the stoichiometric coefficient. The general expression for the momentum transfer for the phase *p* is:

$$S_p^{\vec{U}} = \dot{r}\left(\sum_{pr_p} s_{pr_p} M_{pr_p} \vec{U}_{net} - \sum_{r_p} s_{r_p} M_{r_p} \vec{U}_{r_p}\right) \tag{19}$$

For the specific reaction path (10) considered, one obtains:

$$S_l^{\vec{U}} = \dot{r}\left(M_P \vec{U}_{net} - M_{Na}\vec{U}_l\right) \tag{20}$$

$$S_g^{\vec{U}} = \dot{r}\left(-\frac{3}{4}M_{CO_2}\vec{U}_g\right) \tag{21}$$

In order to calculate the source term S_p^H, the net enthalpy of the reactants is considered, which is given by:

$$h_{net} = \frac{\sum_r s_r M_r h_r^f}{\sum_r s_r M_r} \tag{22}$$

Where h^f is the enthalpy of formation. It is assumed that this net enthalpy is distributed to the products in the ratio of their mass production rates. Therefore, the heat source term for the phase *p* is given by:

$$S_p^H = \dot{r}\left(\sum_{pr_p} s_{pr_p} M_{pr_p} h_{net} - \sum_{pr_p} s_{pr_p} M_{pr_p} h^f_{pr_p}\right) \quad (23)$$

For the specific reaction path (10), Eqs. (22) and (23) become:

$$h_{net} = \frac{M_{Na} h^f_{Na} + \frac{3}{4} M_{CO_2} h^f_{CO_2}}{M_{Na} + \frac{3}{4} M_{CO_2}} \quad (24)$$

$$S_l^H = \dot{r}\left(M_P h_{net} - M_P h_P^f\right) \quad (25)$$

$$S_g^H = 0 \quad (26)$$

Finally, one species transport equation is required for the Na and *P* liquid mixture. The generalized species conservation equation for a multiphase mixture can be written in the following form:

$$\frac{\partial}{\partial t}\left(\alpha_p \rho_p Y_{i,p}\right) + \nabla \cdot \left(\alpha_p \rho_p \vec{U}_p Y_{i,p}\right) = -\nabla \cdot \left(\alpha_p \vec{J}_{i,p}\right) + S_{i,p} \quad (27)$$

In Eq. (27), $Y_{i,p}$ is the mass fraction of species *i* in the phase *p*, $\vec{J}_{i,p}$ is the diffusion flux of species *i* inside the phase *p* and $S_{i,p}$ is the source term accounting for production or destruction of species *i* in the phase *p*, due to chemical reactions. The Fick's law is used to model mass diffusion due to concentration gradients, under which the diffusion flux can be written as:

$$\vec{J}_{i,p} = -\rho_p D_{i,p} \nabla Y_{i,p} \quad (28)$$

Where $D_{i,p}$ is the mass diffusion coefficient of species *i* in the mixture of phase *p*.

For the Na and *P* liquid mixture, it is chosen to solve the transport equation for the Na species. The mass diffusion coefficient of Na inside the liquid mixture was fixed equal to 10^{-9} $m^2 \cdot s^{-1}$, a typical value for mass diffusion coefficient in liquids. The source term taking into account the chemical reaction is:

$$S_{Na,l} = \dot{r} \cdot M_{Na} \quad (29)$$

5. RESULTS

The Ansys Fluent 14 CFD package was employed to solve the equations described in the previous paragraphs. The numerical model has been applied to a numerical domain representing the CO_2-into-sodium jet test facility built at CEA Cadarache [7]. The goal was to validate the numerical results employing the experimental temperature measurements performed in this facility. The numerical domain represents the experimental facility cylindrical pool: its diameter is 100 mm, and its height corresponds to the sodium level considered, which is 200 mm in the experimental tests. In the center of the bottom face of the computational domain, a 1 mm diameter nozzle is placed; the nozzle length is 2 mm, corresponding to the sonic throat length of the nozzles employed in the experimental tests. The computational domain was filled with an unstructured and tetrahedral mesh featuring 98,000 cells. Initial sodium temperature was 773 K, corresponding to the operative temperature inside the heat exchanger in the hotter region: at

773K, sodium density is 830 $kg \cdot m^{-3}$. Following the experimental results obtained by Gicquel [16], the reaction is supposed to lead to an important increase in temperature: a mean temperature of 873K was retained for fixing a constant sodium density, which, at this temperature, is equal to 800 $kg \cdot m^{-3}$. CO_2 total injection temperature is 748K, its total pressure is 1.0MPa. The corresponding critical (Mach equal to one) CO_2 mass flux was fixed as inlet boundary condition at the nozzle. The CO_2 density is treated with an ideal gas law. A pressure boundary condition, with a constant value of 0.1MPa, was fixed at the top of the cylindrical pool. The turbulent kinetic energy at the inlet is estimated through $k_{in} = \frac{3}{2}\left(U_{mean} \cdot I\right)^2$, where U_{mean} is the mean flow velocity at the inlet and *I* is the turbulence intensity at the inlet (estimated through $I = 0.16 \cdot \mathrm{Re}^{-1/8}$). The turbulence dissipation at the inlet is evaluated through $\varepsilon_{in} = C_\mu^{3/4} \frac{k_{in}^{3/2}}{l}$, where *l* is the turbulence length scale (estimated through $l = 0.07 \cdot d_{nozzle}$).
Following Epstein's correlation [11] and Eq. (8), the estimated droplet and bubble diameters were 20 μm and 0.4 mm, respectively. The bubble diameter was calculated through non-reactive jet simulations, using the turbulent dissipation rate calculated by the model, in the region downstream the gas injection where the void fraction approaches the highest limit of bubbly regime void fraction. Following the results in [6], the droplet-flow lowest void fraction limit was fixed equal to 0.80, and the bubbly-flow highest void fraction limit to 0.50.

The numerical stability of a two-fluid computation of an underexpanded gas-into-liquid jet is a critical aspect: the supersonic Mach numbers reached are critical for the numerical stability of pressure–velocity coupling algorithms. In Ansys Fluent, the Phase Coupled SIMPLE (PC-SIMPLE) algorithm developed by Vasquez and Ivanov [17] is employed for the pressure-velocity coupling. This solver has proven stable calculations for underxpanded non-reactive gas-into-liquid jets [6]. Nevertheless, the additional source terms (detailed in the section 4) included in each equation, for taking into account the heterogeneous chemical reaction, further increase the complexity of the numerical formulation. One direct consequence is the fact that acceptable numerical convergence could not be achieved adopting a spatial discretization order higher than one. Therefore, first order upwind had to be adopted for the spatial discretization of each equation. Implicit temporal scheme was employed, with time step ranging from 10^{-5} to 10^{-4} seconds. The chemical reaction was implemented inside the numerical calculation using the Stiff Chemistry Solver, available in Ansys Fluent: for each time step, all the equations are first solved spatially with the reaction rate set to zero; in the second fractional step, the reaction term is integrated in every cell using a stiff Ordinary Differential Equation solver. This method has shown to guarantee a higher numerical stability than the case of directly taking into account the reaction rate in the calculation.

Numerical simulations were run for different kinetics of reaction: considering Eq. (11), the activation energy of the reaction (9) was fixed equal to $4 \cdot 10^4\ J \cdot mol^{-1}$ (following the results obtained by Gicquel [16]), whereas the pre-exponential factor was the parameter changed in order to obtain different reaction rates. Fig. 2 shows the numerical axial temperatures and void fraction profiles, as a function of the pre-exponential factor of the Arrhenius equation. The simulations were stopped at the time when steady state solution was achieved. As expected, the increasing of the chemical reaction rate leads to an increasing of the maximum temperature value, and a shift of the maximum temperature peak and the complete gas consumption point towards the nozzle, as it can be observed in Fig. 2. As expected, the liquid phase temperature is higher than the gas phase temperature, since no enthalpy is transferred to the gas phase by the chemical reaction (the source term (26) is zero); it is the liquid phase that heats the gas phase.
The maximum temperature experimentally found by Gicquel was 1300K at a 4.3 nozzle-diameter distance [16], corresponding to a rise of about 550K, considering the initial sodium and CO_2 temperatures in the experimental tests. Nevertheless, the thermocouple technique employed to measure the temperature by Gicquel is supposed to always provide a stagnation value. If one considers a Mach number of 1-1.5 at a

distance of 4.3 nozzle diameters (this is the order of magnitude of the calculated Mach at this position, see Fig. 4), the static temperature corresponds to about the 80% of the stagnation 1300K measured, meaning that the temperature rise must be reduced to about 300K. The maximum static temperature calculated for the higher pre-exponential factor investigated ($1 \cdot 10^{11}\ m^3 \cdot (mol \cdot s)^{-1}$) corresponds to a temperature rise of 250K in the gas phase (considering the initial CO_2 temperature of 750K) and 330K in the liquid phase (considering the initial sodium temperature of 773K), as it can be observed in Fig. 2.

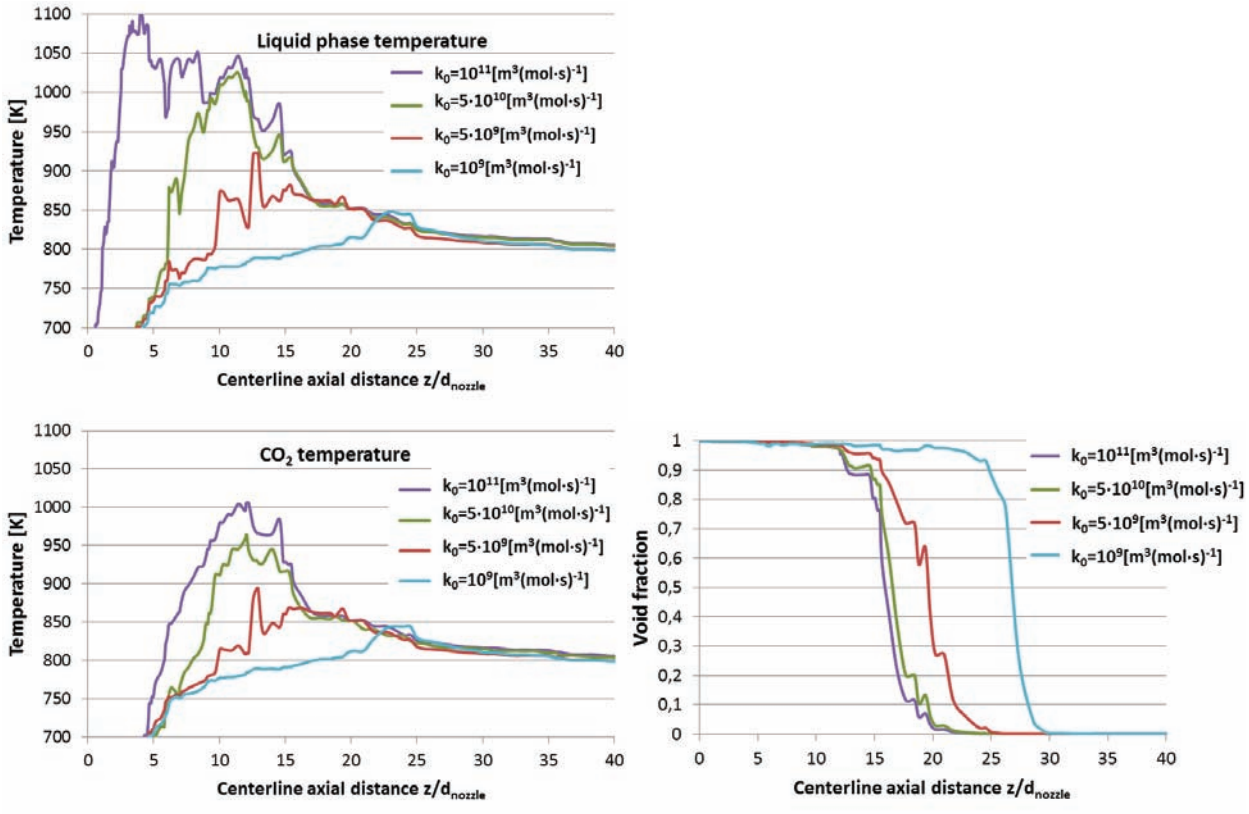

Figure 2: Liquid and gas phase static temperature and void fraction along the jet centerline, as a function of the chemical reaction rate (through the pre-exponential factor k_0).

The peak in the gas static temperature is found at an axial distance of about 11-12-nozzle-diameters, whereas the maximum temperature in the liquid phase is reached at 4-nozzle-diameters. However, looking at the corresponding calculated void fraction profiles reported in Fig. 2, it is likely to assume that, up to a distance of 12-nozzle-diameter distance, the temperature experimentally measured corresponds to the gas phase temperature. The presence of a very little, but not zero, liquid fraction in the region very close to the gas injection, explains the liquid phase temperature peaks calculated in this region: this represents a purely numerical result, meaningless considering that the calculated liquid volume fraction is as low as 0.4% at a 5-nozzle-diameter distance.
Fig. 3 shows the numerical contours of gas and liquid temperature obtained for a pre-exponential factor equal to $5 \cdot 10^{10}\ m^3 \cdot (mol \cdot s)^{-1}$. Fig. 4 shows the gas phase velocity: the underexpansion with gas velocity passing from sonic to supersonic conditions is well calculated by the numerical model. The void fraction and reaction product mass fraction contours are also shown in Fig. 4.

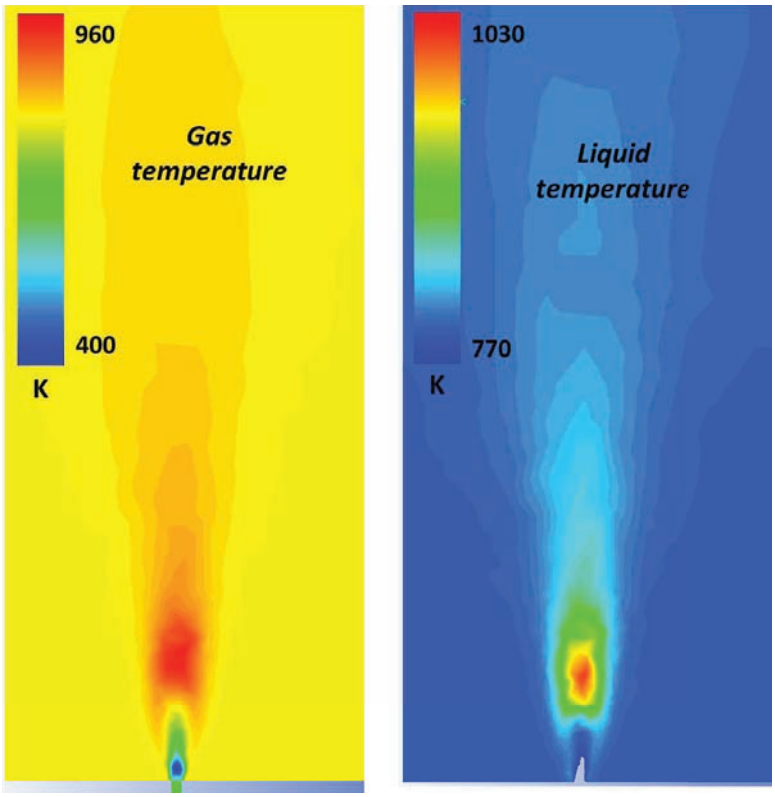

Figure 3: Contours of gas and liquid phase temperature, calculated for $k_0 = 5 \cdot 10^{10}\ m^3 \cdot (mol \cdot s)^{-1}$. For the liquid phase, the region close to the nozzle is out of range (however, one should remember that liquid temperature in this region is meaningless, due to practically zero liquid volume fraction).

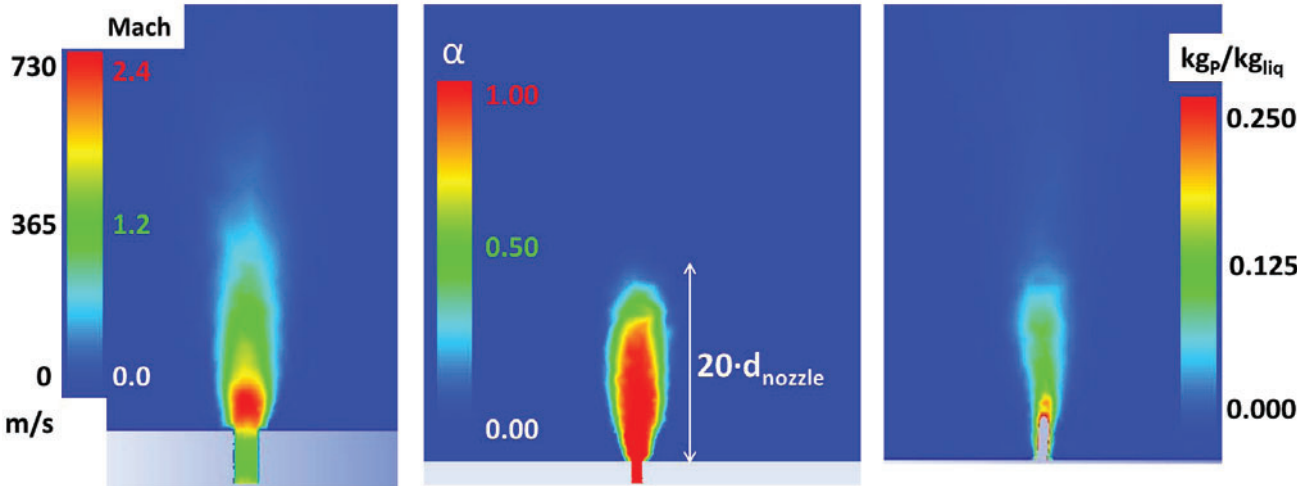

Figure 4: Contours of CO_2 velocity and void fraction, and of liquid species *P* mass fraction, calculated for $k_0 = 5 \cdot 10^{10}\ m^3 \cdot (mol \cdot s)^{-1}$.

5. CONCLUSIONS

A numerical model of the underexpanded reactive CO_2-into-sodium jet, forming as consequence of leakage inside the CO_2-Na heat exchanger of a SFR, has been developed. The model is able to take into account all the relevant physical aspects of this type of two-phase flow, such as the high compressibility effects in the gas phase, the droplet to bubbly flow transition and the heterogeneous chemical reaction between the CO_2 and the sodium. The profiles of void fraction, temperature, velocity and mass fractions can be provided by the numerical model. The present model has already been applied to a real Na- CO_2 typical shell&tube heat exchanger: critical information such as the temperature profiles on the stainless steel tubes can be predicted, as well as the distribution of the reaction products, which is important to investigate if the solid products can cause plugging issues in sensible parts of the heat exchanger. This model will contribute to understand the potentialities of supercritical-CO_2 cycles for SFRs.
Moreover, the present model can be easily adapted to the investigation of other jets, such as the steam-into-sodium jets forming as a consequence of an accidental leakage inside the steam generator of a SFR coupled with a steam Rankine cycle.

ACKNOWLEDGMENTS

Authors would like to thank Sergio Vasquez-Malebran and Denis Tschumperlé of ANSYS for their precious and essential technical support.

REFERENCES

1. N. Alpy et al. Gas cycle testing opportunity with ASTRID, the French SFR prototype. In Supercritical CO_2 Power Cycle Symposium, May 24-25 (2011) Boulder, Colorado.B.C.
2. J. Floyd et al. A numerical investigation of the sCO2 recompression cycle off-design behaviour, coupled to a Sodium cooled Fast0 Reactor, for a seasonal variation in the heat sink temperature. Nuclear Engineering and Design, 260:78 (2013).
3. Yoonhan Ahn and Jeong Ik Lee. Study of various Brayton cycle designs for small modular sodium-cooled fast reactor. Nuclear Engineering and Design, 276:128 (2014).
4. Woo Seok Jeong, Jeong Ik Lee, and Yong Hoon Jeong. Potential improvements of supercritical recompression CO2 Brayton cycle by mixing other gases for power conversion system of SFR. Nuclear Engineering and Design, 241:2128-2137 (2011).
5. J.H. Eoh et al. Wastage and self-plugging by a potential CO_2 ingress in a supercritical CO_2 power conversion system of an SFR. Journal of NUCLEAR SCIENCE and TECHNOLOGY, 47:1023-1036 (2010).
6. D. Vivaldi, F. Gruy, N. Simon, and C. Perrais. Modelling of a CO_2-gas jet into liquid-sodium following a heat exchanger leakage scenario in Sodium Fast Reactors. Chemical engineering research and design, 91:640-648 (2013).
7. L. Gicquel et al. Supercritical CO_2 brayton cycle coupled with a sodium fast reactor: Na/ CO_2 interaction experiments and modeling. In International Congress on Advances in Nuclear Power Plants 2010 (ICAPP 2010) San Diego, California, USA, 13-17 June 2010.
8. S. Sarkar et al. The analysis and modeling of dilatational terms in compressible turbulence. Journal of Fluid Mechanics, 227:473-493 (1991).
9. Y. Tobita et al. Interfacial area modeling for a multiphase, multicomponent fluid-dynamics code. In Proceedings of The International Conference on Multiphase Flows 91 - Tsukuba, 1991.
10. K. Morita et al. Applications of the SIMMER-III fast reactor safety analysis code to thermal interactions of melts with sodium and water. In 7th International Conference on Nuclear Engineering, Tokyo, Japan, April 19-23, 1999, ICONE-7250, 1999.

11. M. Epstein, H. K. Fauske, and N. Yoshioka. Establishment of analytical model for peak temperature within a sodium-water reaction jet, (II) mean droplet size in a submerged gas jet. Journal of Nuclear Science and Technology, 42:961-969 (2005).
12. H. Kudoh et al. Visualization on the behavior of inert gas jets impinging on a single glass tube submerged in liquid sodium. Journal of Nuclear Science and Technology, 50:72-79 (2013).
13. J.O. Hinze. Fundamentals of the hydrodynamic mechanism of splitting in dispersion processes. AIChE Journal, 1:289–295 (1955).
14. A.N. Kolmogorov. On the disintegration of drops in a turbulent flow. Dokl.Akad. Nauk. SSSR, 66:825–828 (1949).
15. D. Vivaldi., F. Gruy, and C. Perrais. A numerical model for the CO_2-sodium chemical interactions in Sodium Fast nuclear Reactors. Chemical Engineering Research and Design, 96:121-129 (2015).
16. L. Gicquel. Etude des mécanismes et cinétiques des interactions sodium CO2. Contribution à l'évaluation d'un système de conversion de l'énergie au CO_2 supercritique pour les réacteurs rapides à caloporteur sodium. PhD thesis, 2010.
17. S.A. Vasquez and V.A. Ivanov. A phase coupled method for solving multiphase problems in unstructured meshes. In Proceedings of ASME FEDSM00: ASME 2000 Fluids Engineering Division Summer Meeting, Boston.